Statistical analysis of the plasmoid evolution with Geotail observations

A. Ieda,[1] S. Machida,[1] T. Mukai,[2] Y. Saito,[2] T. Yamamoto,[2] A. Nishida,[2] T. Terasawa,[3] and S. Kokubun[4]

Abstract. Plasmoids in the Earth's magnetotail were studied statistically, using low energy particle (LEP) and magnetic field (MGF) data from the Geotail spacecraft. Their evolution along the tail axis from $X_{GSM'} = -16$ to $-210\,R_E$ was investigated with 824 plasmoid events. Their dependence on $Y_{GSM'}$ was studied as well to derive the three-dimensional structure of the plasmoids. (The coordinates are aberrated to remove the average effects of the orbital velocity of the Earth about the Sun.) We defined a plasmoid as a structure with rotating magnetic fields and enhanced total pressure. In the near tail ($X_{GSM'} \geq -50\,R_E$), there was a tendency for the plasmoids to be observed in the premidnight sector around the tail axis ($|Y_{GSM'} - 3| \leq 10\,R_E$), while they were observed widely ($|Y_{GSM'}| \leq 20\,R_E$) in the middle tail ($-50 > X_{GSM'} \geq -100\,R_E$) and in the distant tail ($-100\,R_E > X_{GSM'}$). The plasmoids expanded in the $\pm Y_{GSM'}$ direction with typical velocities of $\pm 130 \pm 100$ km/s in the near tail. This strongly supports the view that plasmoids are initially formed at the near-Earth neutral line which has a limited extent in the $Y_{GSM'}$ direction. The plasmoids accelerated in the downtail direction from 400 ± 200 km/s to 700 ± 300 km/s from the near to the middle tail. Then, it is suggested that they decelerated to 600 ± 200 km/s as they traveled to the distant tail. The ion temperature inside plasmoids was 4.5 ± 2 keV in the near and middle tail, and then rapidly decreased to 2 ± 1 keV from the middle to the distant tail region. The ion temperature in the distant tail was 2 times higher than the values deduced previously. Typical plasmoid dimensions were estimated to be $10\,R_E$ (length) $\times 40\,R_E$ (width) $\times 10\,R_E$ (height) in the middle and distant tail. The energy carried by each plasmoid was $\sim 2 \times 10^{14}$ J in the middle tail, half of which was lost from the middle to the distant tail. Inside plasmoids, the thermal energy flux exceeded the bulk energy flux and Poynting flux. The energy released tailward in the course of a substorm was estimated to be roughly 10^{15} J.

1. Introduction

Hones [1976] applied the magnetic reconnection theory to magnetic substorm phenomena and proposed the "near-Earth neutral line" (NENL) model, which is now widely accepted as one of the most successful candidates to explain the release and transport of stored energy in the magnetotail [*Baker et al.*, 1996]. The fast tailward flow with a developed magnetic loop structure from the NENL is known as a plasmoid [*Hones et al.*, 1984a, b]. Observations of plasmoids are highly correlated with substorm onsets in view of magnetic field data observed at ground stations and energetic particle data from geosynchronous satellites [*Moldwin and Hughes*, 1993; *Nagai et al.*, 1994]. In the tail lobe, a traveling compression region (TCR) is often observed and is interpreted to be a remote manifestation of a plasmoid passage [*Maezawa*, 1975; *Slavin et al.*, 1993].

Previous quantitative studies concluded that (1) average electron density and temperature of plasmoids were 0.16 cm^{-3} and 0.18 keV [*Moldwin and Hughes*, 1992a]. Ion temperature was often deduced to be ~ 1 keV [*Scholer et al.*, 1984; *Slavin et al.*, 1993]. (2) The tailward bulk speed of plasmoids was 600-700 km/s [e.g., *Scholer et al.*, 1984; *Richardson et al.*, 1987]. (3) Earlier studies found that plasmoids had a scale length of 50-150 R_E in the X_{GSM} direction [e.g., *Hones et al.*, 1984b; *Richardson et al.*, 1987]. On the other hand, *Moldwin and Hughes* [1992a] (hereinafter referred to as MH92) reported a shorter length of only 17 R_E. It is notable

[1] Department of Earth and Planetary Science, Kyoto University, Kyoto, Japan.

[2] Institute of Space and Astronautical Science, Sagamihara, Kanagawa, Japan.

[3] Department of Earth and Planetary Physics, University of Tokyo, Hongo, Tokyo, Japan.

[4] Solar Terrestrial Environment Laboratory, Nagoya University, Toyokawa, Aichi, Japan.

that the length of TCR was estimated to be 35 R_E by *Slavin et al.* [1993] (hereinafter referred to as S93). This value was regarded to represent the length of the bulge portion of the fast flow. This difference in lengths is primarily due to the variety in the identification of plasmoids' boundaries.

The evolution of plasmoids from $X_{GSM} \approx -50$ to $\sim -240\, R_E$ was statistically studied by MH92 with electron and magnetic field data observed by the ISEE 3 spacecraft. *Moldwin and Hughes* [1992b] made a case study, in which the same plasmoid was investigated with magnetic field data observed by the IMP 8 spacecraft at $X_{GSM} = -30.4\, R_E$ and electron and magnetic field data by ISEE 3 at $X_{GSM} = -168.2\, R_E$. The two papers above concluded that the plasmoids remained relatively stable: Their size, velocity, and magnetic field structure remained fairly constant as they propagated downtail from the near tail to the distant tail.

Plasmoids are thought to be one of the major constituents of magnetic substorms. Their roles in the energy transport during substorms must be clarified quantitatively to check the NENL model. Pictures of plasmoids have been restricted to the noon-midnight meridian plane. Dependence on the downtail distances has also been less clear due to the lack of high-resolution ion thermal data and the small number of plasmoids studied. The goals of this paper are to determine the characteristics and quantities of plasmoids with distance across and down the tail, to discuss the three-dimensional structure of plasmoids and their evolution along the tailward direction, and also to estimate the dimensions of plasmoids and the energy transported by plasmoids in association with substorm energetics.

2. Instruments and Data Set

The Geotail spacecraft was planned to conduct an extensive survey of the magnetotail beyond the lunar orbit as well as in the near-Earth tail region [*Nishida*, 1994]. The early phase of the Geotail mission concentrated on the study of the deep tail region down to $X_{GSM} \approx -210\, R_E$, since Geotail was launched on July 24, 1992. From November 1994, the emphasis changed, turning Geotail into near-Earth orbits, and this data collection was completed in a few months. Since then, Geotail has continued the survey of the near-Earth magnetotail ($-10 > X_{GSM} \geq -30\, R_E$) in the latter phase.

The low energy particle (LEP) instrument on board Geotail was designed to carry out three-dimensional plasma measurements [*Mukai et al.*, 1994]. The three-dimensional velocity distribution functions of ions and electrons are obtained for each spin (approximately 3 s). In this study, we used 12-s (four-spin period) averages of the distribution function and velocity moments of ions. We calculated ion velocity moments on the assumption that all ion species are protons. The calculated densities were routinely (but this was not always possible) compared with those estimated from the plasma wave instrument (PWI) data, that is, the lower cutoff frequencies of the continuum radiation. We es-

timate that the ion parameters used in this study are accurate within ±10% for density and velocities and within 10-20% for ion temperatures.

We also used magnetic field data obtained by the magnetic field (MGF) experiment, which was described in detail by *Kokubun et al.* [1994]. Measured vector magnetic fields were transmitted to the ground at a rate of 16 samples per second. We used each-spin-averaged data to identify plasmoids and four-spin-averaged data (approximately 12-s values) for the statistical study in the present analysis.

3. The Selection Criteria for Plasmoids

3.1. Definition of Plasmoid

There seems to be some confusion regarding the term "plasmoid" in the magnetotail, and we would like to clarify this definition in this paper. One source of confusion is that the term plasmoid has been used both for whole fast bulk flow and for an elementary structure. We defined plasmoid as the latter. Historically, *Hones et al.* [1984b] found that the fast flow consists of a plasmoid with a looped magnetic field and the separatrix layer with interplanetary field lines. Later, *Richardson et al.* [1987] divided the separatrix layer into two layers and called them the postplasmoid plasma sheet (post-PPS) with high-β plasma, and the plasma sheet boundary layer (PSBL) with low-β plasma. In addition to these elements, there also exists the plasma sheet ahead of the plasmoid, activated by an approaching plasmoid as shown in Figure 1. We will call this precursor region the preplasmoid plasma sheet (pre-PPS), examples of which will be presented later.

More confusion results from the magnetic topology of a plasmoid. In earlier works, plasmoids were thought to have closed-looped magnetic field lines [e.g., *Hones*,
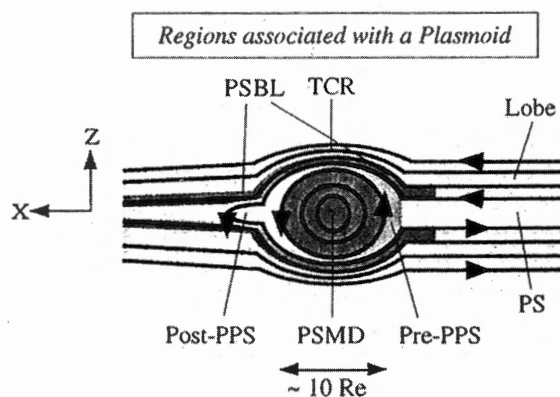
Figure 1. Sketch (noon-midnight cross section) illustrating regions associated with a plasmoid event. Plasmoid events consist of a plasma sheet boundary layer (PSBL), a preplasmoid plasma sheet (pre-PPS), the plasmoid itself (PSMD), and a postplasmoid plasma sheet (post-PPS). In the tail lobe region, a traveling compression region (TCR) is observed as the signature of plasmoid passage. Ahead of these regions, there still exist a relatively quiet tail lobe (lobe) and plasma sheet (PS). The solid lines show the magnetic field lines.

Total Pressure distribution

$$\mathbf{J} \times \mathbf{B} - \nabla P_p = 0$$
$$\Leftrightarrow$$
$$-\nabla(P_p + P_b) = \mathbf{Fmt}$$

Pp : Thermal Pressure
Pb : Magnetic Pressure
Pt = Pp+Pb : Total Pressure
Fmt : Magnetic Tension

Reversal magnetic field

$-\nabla P_p \quad -\nabla P_b$
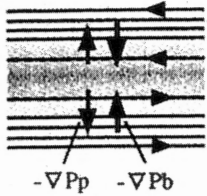
Total pressure is constant
(Pressure Balanced)

Helical or Closed Loop

$-\nabla Pt \quad Fmt$
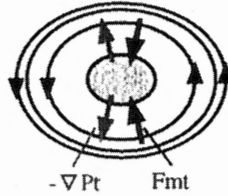
Total pressure
is _enhanced_ inside the loop
(_not_ Pressure Balanced)

Figure 2. Illustration of the equilibrium state and the total pressure distribution in (left) the quiet plasma sheet and in (right) a plasmoid. Solid lines are the magnetic field lines in the noon-midnight meridian plane.

1976]. It is unlikely, however, that the "legs" of the magnetic loop ever interconnect with themselves to form a fully detached "magnetic island." Later, it was demonstrated that most plasmoids have helical magnetic field structures, called "flux ropes" [e.g., *Hughes and Sibeck*, 1987]. It is likely that magnetic islands are relatively rare and are limiting cases of magnetic flux ropes. Currently, the term plasmoid is sometimes used for a closed magnetic field structure (magnetic island) to emphasize its difference from a helical magnetic field structure (flux rope) in some papers, while in some cases, plasmoid means both of these. We defined plasmoid comprehensively as the latter.

3.2. Total Pressure Enhancement Inside a Plasmoid

We would like to discuss the total pressure inside a plasmoid before listing criteria used in this study. The total pressure (P_t) is defined as the sum of the thermal pressure of the plasma (P_p) and the magnetic pressure (P_b). Total pressure distributions inside two typical quasi-equilibrium states are schematically illustrated in Figure 2, where a quiet plasma sheet in the magnetotail is shown on the left. As the magnetic tension force (F_{mt}) is negligible, the total pressure is constant from the tail lobe to the center of the plasma sheet. However, this is not the case for a plasmoid, as shown on the right of Figure 2. The total pressure inside the plasmoid must be higher than that in the background because magnetic tension force acts to compress the plasmoid. Therefore a total pressure enhancement (TPE) is a necessary condition for plasmoids. If TPE is mainly due to the enhancement of plasma pressure, the plasmoid can be categorized to be the magnetic-island type. If it is due to the enhancement of magnetic pressure, the plasmoid can be categorized to be the flux-rope type.

Although the plasmoid drawn in Figure 2 is a magnetic-island type, the discussion above can also be applied to a flux-rope-type plasmoid.

In the tail lobe region, the magnetic field magnitude is also expected to be enhanced, mainly by compression (not by magnetic tension), because a plasmoid is thicker than a quiet plasma sheet: S93 used magnetic field magnitude enhancement in excess of 1% of the lobe field magnitude for a criterion of TCR. In the case of a plasmoid itself, the magnetic tension further enhances the total pressure. The increase of the total pressure is sometimes comparable to or even slightly larger than the baseline value in clear plasmoid events, as shown later. However, since it is not usual for a spacecraft to pass through the center of a plasmoid, the actual observed TPE is often weaker.

An advantage of using TPE as a criterion in selecting plasmoids is that we can then exclude some types of nonplasmoid events. It is commonly accepted that a north-then-south turning of the magnetic field indicates the existence of a plasmoid and supports the NENL model. However, there is another possibility that such magnetic field variations do not mean plasmoids but waves (possibly normal mode waves) [*Lee et al.*, 1988]. The existence of plasmoids is supported by the fact that the north-then-south turning events are observed 2.5 times more often than the south-then-north events [*Tsurutani et al.*, 1987]. However, it also means that about 30% of north-then-south turning events may not signify plasmoids but normal mode waves, or even something else. In normal mode waves, the total pressure at the inner region (plasma sheet site) is lower than that of the outer region (tail lobe site), as pointed out by *Slavin et al.* [1989]. Therefore we can exclude normal mode wave events by adding the TPE criterion.

3.3. Selection Criteria

We have visually scanned the data plots and identified plasmoid events using the following criteria, which includes a TPE condition unique to our study.

1. A TPE in excess of 10% of the baseline value was required. The smaller values of the total pressure at the boundaries of the plasmoids were selected as the baselines. The boundary identifications will be described later. The contribution of electrons to the thermal pressure was omitted in the calculation of the total pressure.

2. Only tailward moving plasmoids with a maximum tailward speed faster than 200 km/s were selected. Although we found some events which could be interpreted as stagnant or earthward flowing plasmoids, we excluded them for simplicity.

3. The existence of a B_z bipolar signature, with a peak to peak amplitude greater than 2 nT, was also required. Although a small number of plasmoids with only a B_y bipolar signature might exist as a consequence of twisting of the magnetotail in some types of solar wind conditions, we excluded these for simplicity. The reason for the restriction on the amplitude is because a weak magnetic field in the neutral sheet is often wavy, as pointed out by MH92. This may be coincident with

the total pressure enhancement, caused not by the magnetic tension, but rather by the change in solar wind conditions. If this kind of total pressure enhancement is coincident with the large-amplitude B_z bipolar signatures caused by the flapping motion of the magnetotail and with a fast flow in the plasma sheet, they should not be excluded in our criteria. However, such cases seem rare.

4. $N_{i,\max} < 1 \, \text{cm}^{-3}$ and $T_{i,\min} > 0.2$ keV were required to guarantee the region as being inside the plasma-sheet-like region. It is not necessary for the maximum or minimum value to be coincident with the peak of the total pressure.

5. It sometimes happened that Geotail made short excursions from the tail lobe into plasmoids. We excluded such TCR-like cases by using $\beta_{i,x,\max} \geq 1$, where $\beta_{i,x,\max}$ is the maximum of the ratio of the ion thermal pressure to the X component of the magnetic pressure.

The boundaries of plasmoids were identified primarily by identifying the start and the end of TPE, because the total pressure must be enhanced inside the rotating magnetic field structure, as discussed earlier. The center of plasmoids was defined as the inflection point in the north-then-south variation in B_z. Energy time diagrams of ion and electron were often used to identify and exclude PSBLs, in which a high-energy component and a cold drifting component coexist, as described by *Machida et al.* [1994]. We also defined pre-PPS as a constituent of a plasmoid event but excluded it, as well as post-PPS, in the calculations of the plasmoid length. We only selected plasmoids for which we had both ion and magnetic field data without any serious data gaps. Although plasmoids often appeared as multiple events, possibly due to multiple onset substorms, in this paper we did not distinguish between isolated and multiple events.

3.4. Coordinate System

In this study, the aberrated geocentric solar magnetospheric (GSM') coordinate system was used, in which the average effects of the orbital velocity of the Earth about the Sun were removed: All satellite locations and data were aberrated and tilt-corrected with an angle of 4° (the corresponding solar wind speed is 426 km/s) and with a hinging distance of $10 \, R_E$. We usually denoted these as "$X_{\text{GSM}'}$" or "V_x", etc., in this paper. We defined the region $-16 > X_{\text{GSM}'} \geq -50 \, R_E$ as the near tail, $-50 > X_{\text{GSM}'} \geq -100 \, R_E$ as the middle tail, and $-100 > X_{\text{GSM}'} \geq -210 \, R_E$ as the distant tail. The dividing distances were selected on the basis of differences of the typical plasmoid quantities, which will be presented later. We also call the region of $|Y_{\text{GSM}'}| \leq 10 \, R_E$ as the central region and $|Y_{\text{GSM}'}| > 10 \, R_E$ as the flank region.

4. Case Studies

Figure 3 shows three examples of plasmoids at $X_{\text{GSM}'} = -29 \, R_E$ (near-tail case), $-95 \, R_E$ (middle-tail case), and $-199 \, R_E$ (distant-tail case). Figure 3a shows an example of a plasmoid observed in the near tail around 1826 UT on December 10, 1994. Thirty minutes of data are shown in the GSM' coordinates. The top five panels consist of magnetic field data (in nanoteslas) for total strength, its components, and root-mean-squares of the magnetic field fluctuations. The next panel is ion beta (β_i), which is the ratio of ion thermal pressure (P_i) to magnetic pressure (P_B). In the next panel, $P_B + P_i$ is superposed on P_i. Since electron pressure is negligible, β_i and $P_B + P_i$ are thought to be plasma beta and total pressure, respectively. The other five panels are ion moments of the density (per cubic centimeter), temperature (keV), and the three components of velocity in km/s. Universal time and satellite locations are shown at the bottom of the figure. The solid vertical lines marked S, C, and E at 1826:14 UT, 1826:46 UT, and 1827:30 UT are the start, center, and the end of the plasmoid, respectively.

At 1826:14 UT (S), total pressure began to rise and reached a peak value at 1826:46 UT (C). This was coincident with the turning of B_z and the peak of B_y in this case, but this is not always the case. B_x was also enhanced, indicating that spacecraft passed slightly off the center of the plasmoid in terms of $Z_{\text{GSM}'}$. Then total pressure decreased down to nearly the background level at 1827:30 UT (E). The interval from S to E is identified as a plasmoid. Inside the plasmoid, V_x was -480 km/s and V_y was 329 km/s, on the average. Since the satellite was located on the dusk side, the significant value of V_y suggests an expansion of the plasmoid in the $Y_{\text{GSM}'}$ direction. One notable point is that inside clear flux-rope-type plasmoids, the thermal pressure is often nearly constant, as seen in this example. Since the gradient of thermal pressure can be negligible, the force-free assumption is valid, even when the plasma beta is as high as unity, as it was in this case.

An example of a plasmoid observed in the middle tail is shown in Figure 3b, in the same format as Figure 3a. Geotail was in the magnetotail at GSM' $(-94.9, -3.1, -1.8) \, R_E$ at 1150 UT on January 16, 1994. The flow was earthward until 1146:57 UT, and then, slow tailward or essentially stagnant until 1148:35 UT (S), and finally, tailward and fast. This sequence is typical in the middle tail. It is also sometimes observed in the near and even in the distant tail, as shown in the previous and in the next examples. The change from a slow to fast tailward flow was explained as follows [*Nishida et al.*, 1994]: The burst flow due to the NENL pushes the ambient plasma ahead, observed as the slow flow, and the following arrival of the burst flow itself is observed as the fast flow. The region with this slow flow is called pre-PPS in this paper. The prior earthward flow can be interpreted to mean that the distant neutral line has become activated before a substorm onset [*Nishida et al.*, 1986]. Inside the plasmoid (between S and E), V_x was -855 km/s and V_y was 125 km/s, on the average.

Figure 3c presents an example of a plasmoid observed in the distant tail, in the same format as Figure 3a. Geotail was at GSM' $(-198.6, 7.3, 7.4) \, R_E$ at 0010 UT on April 18, 1994. Inside the plasmoid, V_x was -204
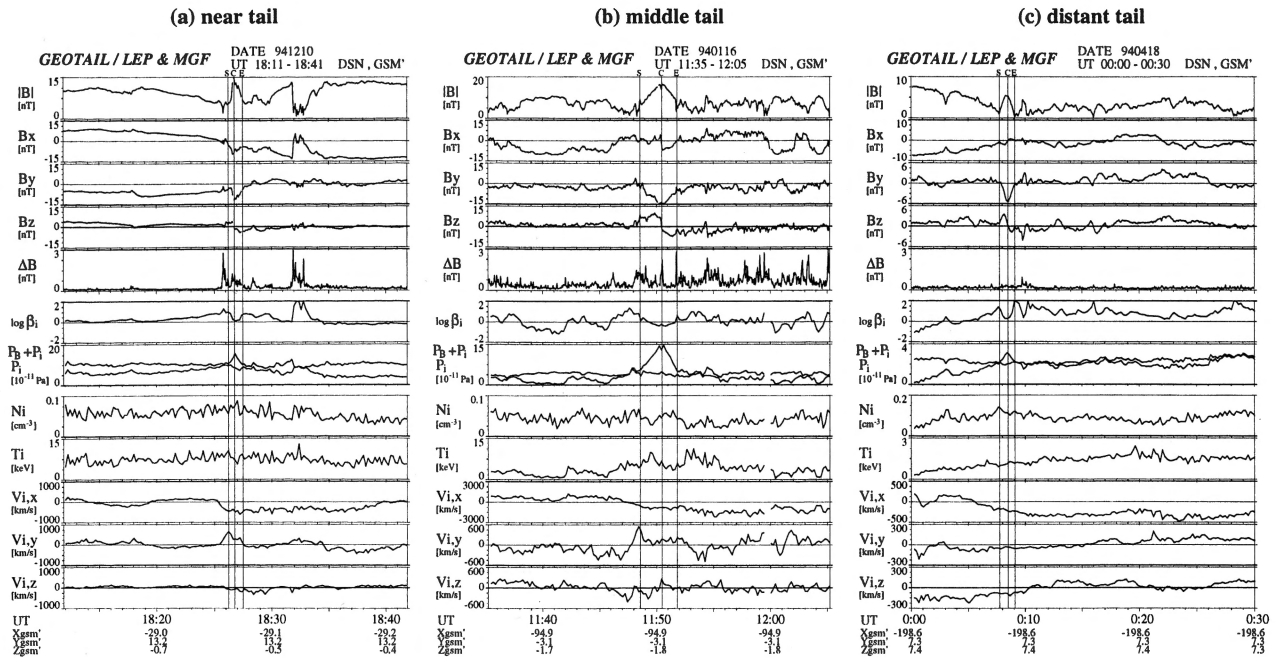
Figure 3. Examples of plasmoids (a) in the near tail, (b) in the middle tail, and (c) in the distant tail. Thirty minutes of magnetic field and ion velocity moments are shown in the aberrated geocentric solar magnetospheric (GSM′) coordinates. Solid vertical lines mark the start (S), center (C), and the end (E) of the plasmoid. The top five panels show 3-s magnetic field data: (from top to bottom) strength, the three components, and root-mean-squares of the magnetic field fluctuations. The next two panels are 12-s averages of ion beta (ratio of ion thermal pressure to magnetic pressure) and pressures (ion pressure and total pressure are superposed). Electron thermal pressure is neglected in the calculation of total pressure. The remaining five panels are 12-s averages of ion velocity moments: ion density (per cubic centimeter), ion temperature (keV), and the three components of velocity (km/s). Also shown on the horizontal scale in the bottom are universal time and the positions of the spacecraft in the aberrated GSM coordinates.

km/s and V_y was −45 km/s. Variations in total and ion thermal pressures were similar to those in the preceding two cases. After the passage of the plasmoid, another B_z bipolar signature was observed around 0016 UT, which was not another plasmoid but rather turbulence behind the plasmoid, because the total pressure was not enhanced inside it.

5. Geotail Orbit and Occurrence Frequencies of Plasmoids

In Figure 4a, the Geotail orbits for the time interval of this study, from September 14, 1993, to March 5, 1996, are displayed in the GSM′ XY plane. The Geotail orbits are also projected in the GSM′ YZ plane for the near tail in Figure 4b, for the middle tail in Figure 4c, and for the distant tail in Figure 4d. It is seen in Figures 4b, 4c, and 4d that the Geotail orbits in the magnetotail were basically restricted to the nominal equatorial plane.

Figure 5a shows the locations of 824 plasmoid events consistent with our selection criteria. Each circle represents the location of one event. The numbers of these events are normalized to the amount of time of Geotail observations in $|Z_{GSM'}| \leq 10\,R_E$. The resultant occurrence frequencies per day in each $10\,R_E \times 10\,R_E$ mesh
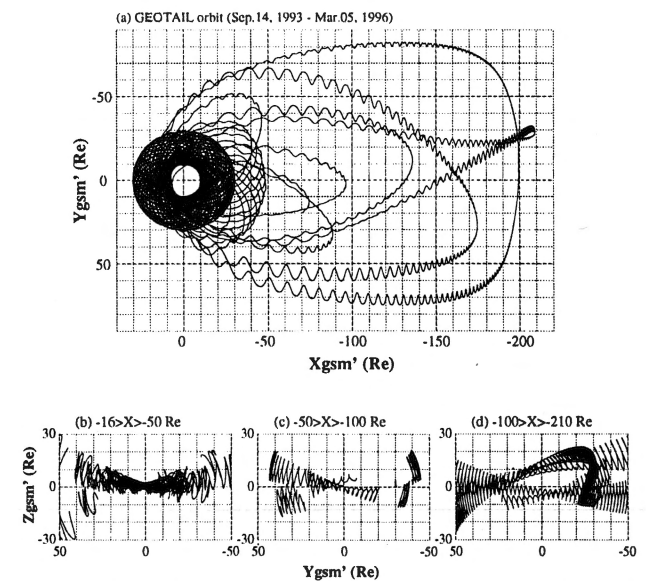
Figure 4. The orbits of the Geotail spacecraft in the aberrated GSM coordinates for the period from September 14, 1993, to March 5, 1996. A hinging distance of $10\,R_E$ and an aberration of 4° are assumed. These are projected in the XY plane for (a) the whole period. These are divided and projected in the YZ plane for (b) the near-tail period, for (c) the middle-tail period, and for (d) the distant-tail period.
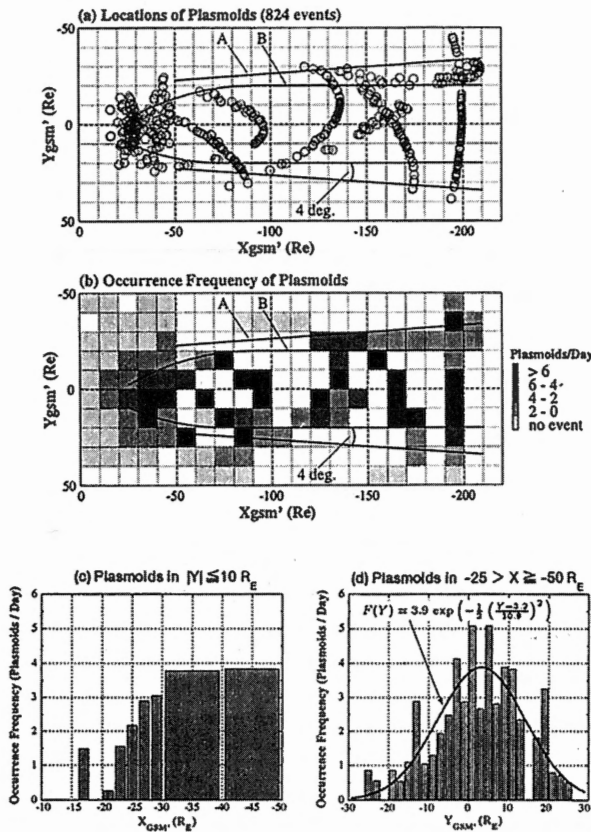
Figure 5. (a) Observed locations of 824 plasmoid events identified in this study are plotted in the GSM$'$ XY plane for the same interval as Figure 4a. Each plasmoid is plotted as a circle. Paired lines A and B are drawn as references. (b) Occurrence frequencies of plasmoid events in each 10 $R_E \times 10$ R_E mesh are plotted as different tones. (c) Occurrence frequencies of plasmoids in the central region of the near tail for a detailed study of the $X_{GSM'}$ dependence. (d) Occurrence frequencies ($F(Y)$) of plasmoids in $-25 > X_{GSM'} \geq -50 R_E$ against $Y_{GSM'}$. A Gaussian-fitted line is also shown by a solid line.

are plotted as different tones in Figure 5b. The regions with the amount of time less than 12 hours are not displayed. In Figure 5b as well as in Figure 5a, two kinds of paired solid lines A and B are drawn as references. Lines A are $Y_{GSM'} = \pm (20 + |X_{GSM'}| \sin 4°)$, which seems to well envelope most plasmoids in the middle and the distant tail. Relatively low occurrence frequencies in the regions between A and B may indicate that these plasmoids were observed when the magnetotail was flapped by solar wind fluctuations and/or when its radius was increased. A flaring of the observable region as marked by lines A supports the suggestion that the tail geometry is undergoing a flapping motion. If the contributions of the flapping motions were removed, it would be expected that the observable region has a width of $\sim 40 R_E$ as marked by lines B in the middle and the distant tail. This width can be interpreted to represent the $Y_{GSM'}$ dimension of the plasmoids.

In the near tail, occurrence frequencies are much lower than those in the middle and the distant tail. The region with relatively high occurrence frequency seems to become wider from the near tail to the middle tail, as marked by lines B. These suggest an expansion of plasmoids in the $\pm Y_{GSM'}$ direction in the near tail, which will be demonstrated later from the study of cross-tail velocity. Although a small number of plasmoids exist in the flank region in the near tail, we rather interpret that plasmoids are localized and that the centers of plasmoids and the NENL are sometimes located in an off-midnight position. The average occurrence frequencies in $-25 > X_{GSM'} \geq -50 R_E$, in the middle tail, and in the distant tail are 2.7, 8.5, and 7.7 (plasmoids/day) in $|Y_{GSM'}| \leq 10 R_E$, and 1.2, 3.5, and 3.9 (plasmoids/day) in $10 < |Y_{GSM'}| \leq 20 R_E$, respectively.

To see the details in the near tail, Figure 5c shows the occurrence frequencies of plasmoids in the central region. The spatial resolution in the $X_{GSM'}$ direction is every $2 R_E$ in $-10 > X_{GSM'} \geq -30 R_E$ and every $10 R_E$ in $-30 > X_{GSM'} \geq -50 R_E$. The amount of observation time is longer than 3 days for each region. Inside $X_{GSM'} \sim -25 R_E$, observations of plasmoids are relatively rare. Therefore it can be concluded that the NENL is usually located earthward of this distance.

Figure 5d shows the occurrence frequencies of plasmoids in $-25 > X_{GSM'} \geq -50 R_E$ with average plasmoid location of $X_{GSM'} = -34 R_E$. The spatial resolution in the $Y_{GSM'}$ direction is every $2 R_E$. The amount of observation time is longer than 1 day for each region except the bin of $-30 \leq Y_{GSM'} < -28 R_E$. It seems that the occurrence frequencies are relatively high in the finite region around the tail axis with their center in the premidnight. A Gaussian-fitted line indicates that the occurrence frequency is relatively high in $|Y_{GSM'} - 3| \leq 10 R_E$. Therefore it can be interpreted that plasmoids have a typical width of $\sim 20 R_E$ with their center at $Y_{GSM'} \approx 3 R_E$ in the near tail. The center of the NENL is also likely to be located at $Y_{GSM'} \approx 3 R_E$.

6. Statistical Study

In this section, we examine the average properties of the plasmoids and compare our results with those found in previous studies. For each plasmoid, representative quantities are calculated by averaging particle and magnetic field data, and then they are averaged in spatially separated bins. In the following, plots of plasma moments and magnetic fields will be shown as functions of the downtail distance and the cross-tail distance. In some figures, quantities reported by MH92 are superposed as the representative result of the ISEE 3 observations.

6.1. Flow Characteristics of Plasmoids

The $X_{GSM'}$ directional velocity (V_x) in plasmoids averaged over every 30-R_E bin as a function of the distance down the tail is shown in Figure 6. The values in the central region and those in the flank region are presented by solid and dotted lines. Error bars indicate the standard deviations. Each plotted $X_{GSM'}$ repre-
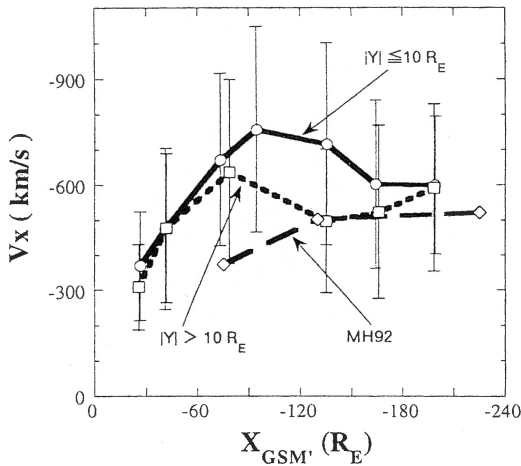
Figure 6. The $X_{GSM'}$ directional velocity of plasmoids (V_x) in the bins of every $30\,R_E$ spatial dimension in $X_{GSM'}$. The solid line represents the V_x of plasmoid observed in the central region ($|Y_{GSM'}| \leq 10\,R_E$). The dotted line corresponds to V_x in the flank region ($|Y_{GSM'}| > 10\,R_E$). The error bars indicate the standard deviation for each bin. The result of *Moldwin and Hughes* [1992a] using ISEE 3 thermal electron measurements is also superposed as a broken line.

sents the average location in the corresponding bin. The data in the flank region from $X_{GSM'} = -90$ to $-120\,R_E$ are not displayed because of the relatively small number of events (11 events).

It was found that from $X_{GSM'} \approx -30\,R_E$ to the middle tail, plasmoids rapidly accelerated, typically from 350 to 700 km/s. In the transition from the middle to distant tail, however, they weakly decelerated with a typical value of 600 km/s. This contradicts the results from the previous studies [e.g., *Gloeckler et al.*, 1984], which showed that plasmoids continue to accelerate through the magnetotail. It has been suggested that the acceleration of plasmoids is due to magnetic draping and dynamic pressure behind a plasmoid [e.g., *Richardson et al.*, 1987], while any interaction with the plasma and magnetic field ahead of them was essentially ignored. We believe that such an interaction is crucial to understand the velocity evolution of plasmoids. In this paper, such interaction regions are called pre-PPS.

It is noted that there was a difference of bulk velocity of typically 100 km/s between the central and flank portion in the distant tail. The value may be reduced from actual ones because of flapping motions. Since this difference continues from $X_{GSM'} \approx -100$ to $\sim -180\,R_E$, plasmoids are expected to deform with a difference of location between the central and the flank portion of typically $10\,R_E$ around $X_{GSM'} = -180\,R_E$.

The results of MH92 are also plotted in Figure 6 as a dotted line, which shows values slower than ours. On the other hand, most of the ISEE 3 results reported in other papers showed results of 600-700 km/s [e.g., *Richardson et al.*, 1987], which agree with our results in the middle and the distant tail. The relatively slower values reported by MH92 possibly stem from their selection criteria: they set no criterion on the speed of a

plasmoid. Our result seems consistent with their results as seen in Figure 10 of their paper.

Figure 7 shows the cross-tail velocity of plasmoids (V_y) in the near, the middle, and the distant tail as functions of $Y_{GSM'}$ with a 10-R_E bin. Regions with sampling numbers smaller than ten are not displayed. Data from the near tail show an expansion of plasmoids in $Y_{GSM'}$ direction, as is evident from the sign of V_y, which was positive in the dusk and negative in the dawn regions. The expansion speed of plasmoids takes a typical value of $V_y = \pm 130$ km/s in the flank region. The expansion of plasmoids in the near tail is consistent with the localization presented previously. The primary cause of the plasmoid expansion is thought to be the enhanced total pressure: Plasmoids are confined by magnetic tension in the $X_{GSM'}$ and $Z_{GSM'}$ directions; however, they are not restricted in the $Y_{GSM'}$ direction until expansion reaches the low-latitude boundary layer. A small offset exists about 20 km/s in the near-tail data. As we have already noted, a plasmoid is preferably located in the duskside ($Y_{GSM'} \approx 3\,R_E$), where the actual offset is expected to be ~ 60 km/s. The offset may indicate the contribution of ions to the diamagnetic current.

There is a similar $Y_{GSM'}$ dependence of V_y in the middle tail, but the magnitude of the velocity in the flank region is only ~ 40 km/s, considerably lower than that in the near tail. However, there is no expansion in the distant tail, which contradicts the results obtained by *Gloeckler et al.* [1984], who suggested that plasmoids expanded with speeds of ± 100 km/s in the distant tail. Although a slight difference of V_y of $\sim \pm 20$ km/s might appear to exist in $|Y_{GSM'}| > 20\,R_E$ in the distant tail, this was interpreted to be due to the unusual directions of the tail axis caused by flapping motions of the tail: Outside of $|Y_{GSM'}| \approx 20\,R_E$, there would be a tendency for plasmoids to be observed in such a condition. Since V_x in the distant tail is typically -600 km/s, a flapping
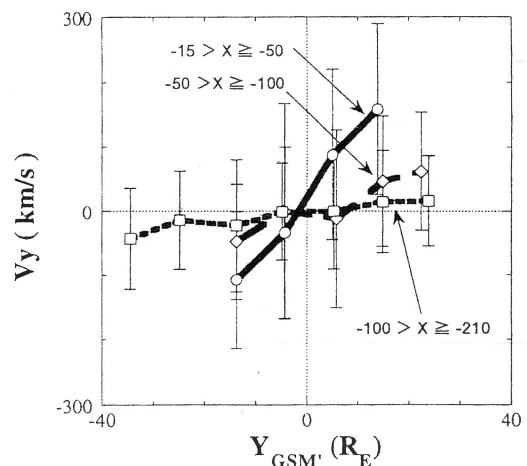
Figure 7. The $Y_{GSM'}$ directional velocity of plasmoids (V_y) in the bins of every $10\,R_E$ spatial dimension in $Y_{GSM'}$. The data sets are also divided into three different regions in terms of $X_{GSM'}$ and shown as three lines. The error bars indicate the standard deviation for each bin.
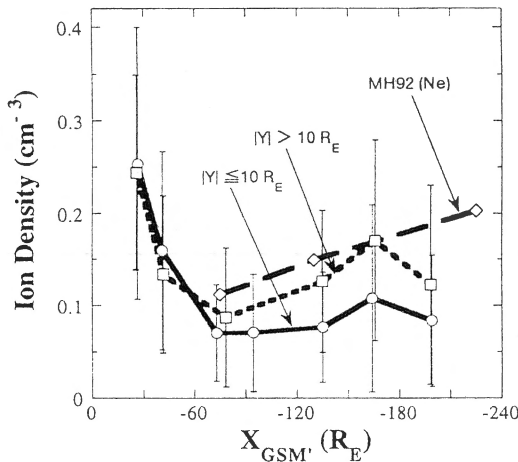
Figure 8. Ion densities of plasmoids against $X_{\text{GSM}'}$ in the same format as Figure 6.

Figure 9. Ion temperatures inside plasmoids against $X_{\text{GSM}'}$. Ion temperatures derived using the ISEE 3 results are also superposed.

motion of the magnetotail with an angle of 4° in the $Y_{\text{GSM}'}$ direction can yield an apparent velocity of ±40 km/s for V_y.

The $Z_{\text{GSM}'}$ directional velocity (V_z) was also investigated. Because of the flapping motions of the tail, we cannot use $Z_{\text{GSM}'}$ directly. If substantial expansion in the $Z_{\text{GSM}'}$ direction exists, we would expect to find it by studying V_z as a function of B_x or β_x (the ratio of the plasma pressure to the $X_{\text{GSM}'}$ component of magnetic pressure). However, there was no relation between V_z and B_x, and no substantial expansion was found in the $Z_{\text{GSM}'}$ direction.

6.2. Other Characteristic Quantities Inside Plasmoids

The density of ions inside plasmoids is shown against $X_{\text{GSM}'}$ in Figure 8. The format is the same as Figure 6. In both central and flank regions, ion density inside plasmoids rapidly decreased, typically from 0.25 to 0.1 cm^{-3} as Geotail went from $X_{\text{GSM}'} \approx -30\,R_E$ to the middle tail. This can be due to the expansion of plasmoids in the $Y_{\text{GSM}'}$ direction between these locations. The density decrease can also occur because the density of the plasma sheet plasma taken into the plasmoid decreases as the plasmoid propagates farther down the tail. After the rapid decrease, the density stayed nearly constant in the central region, while in the flank region it somewhat increased up to 0.15 cm^{-3} in the distant tail. This increase is consistent with the results by MH92 and suggests a mass flux from outside into the flank region, which may be also consistent with the relatively slower plasmoids observed in the flank region.

Figure 9 shows the variation of the ion temperature (T_i) of plasmoids against $X_{\text{GSM}'}$ in the same format as Figure 6. In the central region, the ion temperature was essentially constant and typically 4.5 keV in the near and the middle tail. It rapidly decreased down to 2 keV from the middle to distant tail. Then it became nearly constant in the distant tail. In the flank region, the temperature tended to be somewhat lower.

The variation of ion temperature observed by ISEE 3 is also displayed in Figure 9. Since ISEE 3 only
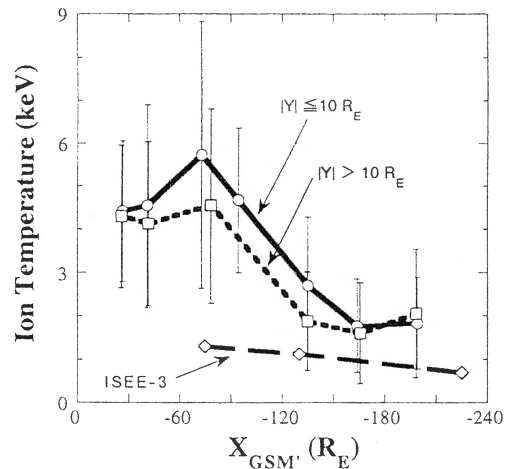
measured the electron temperature (T_e), we assumed $T_i = 5\,T_e$ [*Slavin et al.*, 1985] in producing the plot with T_e as reported by MH92. Ion temperatures inside plasmoids found in this survey were substantially higher than the values deduced from the ISEE 3 results by a factor of 3 in the middle tail and by a factor of 2 in the distant tail. Ion temperature ($T_i \approx 2$ keV) observed by Geotail and electron temperature ($T_e \approx 0.2$ keV) observed by ISEE 3 suggest the ratio of $T_i/T_e \approx 10$ inside plasmoids observed in the distant tail. The high temperature in the middle tail suggests that the NENL remains active, while the mechanism for the rapid decrease of ion temperature in the transition from the middle to distant tail is not yet fully understood. This must be a nonadiabatic cooling because the dimensions of plasmoids do not change significantly, and the density is nearly constant (in the central region) or even somewhat increases (in the flank region) in this transition. It is notable that the locations of the rapid decreases are different for the density and the temperature.

The absolute values of the magnetic field ($|\mathbf{B}|$) were averaged inside plasmoid boundaries and averaged again
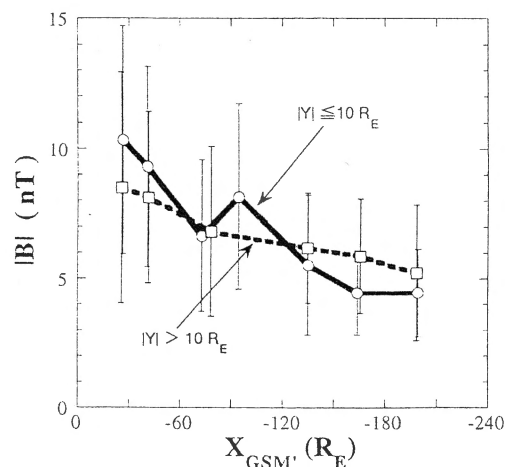
Figure 10. The magnetic field strength inside plasmoids against $X_{\text{GSM}'}$.
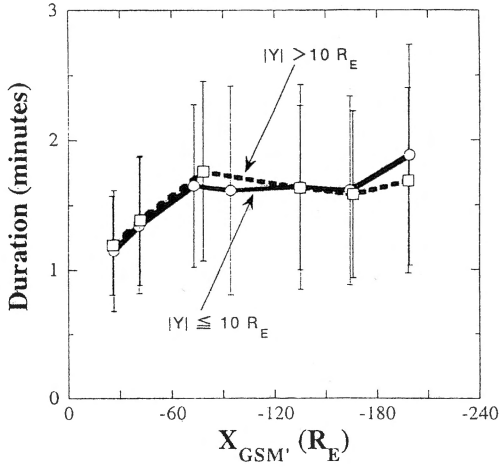
Figure 11.   Duration of plasmoids as a function of $X_{\mathrm{GSM'}}$.

in spatially separated bins. As shown in Figure 10, these monotonically decreased from 10 to 5 nT from the near tail to the distant region, except that there are some fluctuations in the central region. The value ($|\mathbf{B}| \approx 5$ nT) in the distant tail is consistent with previous studies.

Our statistical results on the duration of plasmoids are shown in Figure 11: typically 1 min around $X_{\mathrm{GSM'}} = -30\,R_E$ with an increase to 2 min in the middle and distant tail. The $X_{\mathrm{GSM'}}$ dimensions of plasmoids (L_x) are shown in Figure 12. Calculations were made with the use of the equation

$$L_x = \int_{t_{\mathrm{start}}}^{t_{\mathrm{end}}} |V_x|\,dt \qquad (1)$$

where t_{start} and t_{end} are the times when the frontside and backside boundaries were observed as presented in the three examples shown in Figure 3. L_x derived by (1) is $4\,R_E$ around $X_{\mathrm{GSM'}} = -30\,R_E$ and increases to $10\,R_E$ in the middle and distant tail, possibly due to the pile up of the newly reconnected magnetic field lines in the plasma sheet. Although the duration and lengths of the plasmoids are shorter when comparison is

made with those found in previous studies, the values seem reasonable: the north-south dimension of plasmoids (L_z) is thought to be in the range from a few to $15\,R_E$ [e.g., *Weiss et al.*, 1992; S93] and calculated later to be $\sim 10\,R_E$ in the middle and the distant tail. Since the magnetic tension force tends to make the cross section of a plasmoid circular in the GSM' XZ plane, L_x is expected to be nearly the same as L_z.

6.3. Energy Flux Inside Plasmoids

Figure 13 shows the $X_{\mathrm{GSM'}}$ component of the total and the three components of the energy flux as a function of the downtail distance. The components are thermal ($(5/2)P_i V_x$), kinetic ($(1/2)\rho V^2 V_x$), and electromagnetic or Poynting ($\mathbf{E} \times \mathbf{B}/\mu_0|_x$), where P_i is the ion thermal pressure, ρ is the mass density of plasma, V is the speed of the plasma, $\mathbf{E}$ is the electric field calculated from the velocity and magnetic field with the MHD assumption, and $\mathbf{B}$ is the magnetic field. Electron thermal pressure was neglected in the calculation of the thermal component. As can be seen in Figure 13a, the total energy flux in the central region
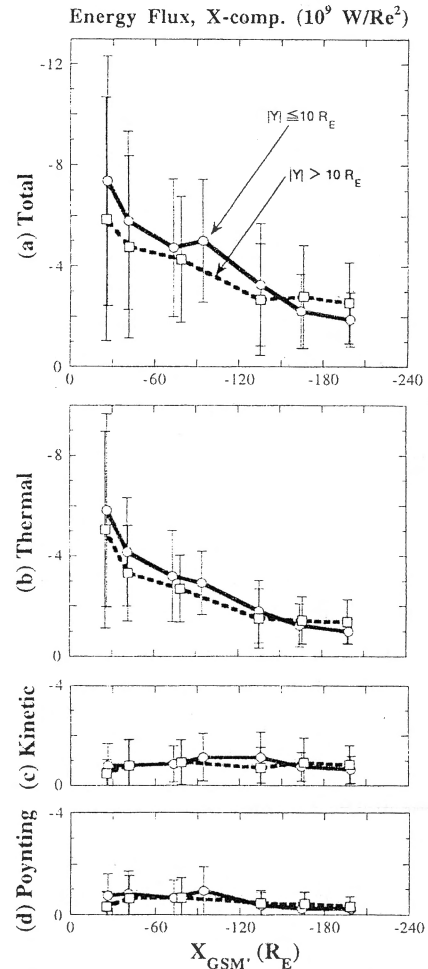
Figure 13.   The $X_{\mathrm{GSM'}}$ component of the energy flux of plasmoids against $X_{\mathrm{GSM'}}$. Figure 13a is the total energy flux inside a plasmoid. Figures 13b, 13c, and 13d are the thermal, kinetic, and Poynting components, respectively. Electron thermal pressure is neglected in the calculation of the thermal component.

Figure 12.   Length of plasmoids against $X_{\mathrm{GSM'}}$.

decreased from $7 \times 10^9 \, \mathrm{W}/R_E^2$ down to $2 \times 10^9 \, \mathrm{W}/R_E^2$ from $X_{\mathrm{GSM'}} \approx -30 \, R_E$ to the distant tail. (The negative values in Figure 13 mean that the flux is tailward). The difference of total energy flux was not very large between the central and the flank region.

From Figures 13b, 13c, and 13d, it is seen that the ratios of the three components of energy fluxes were (thermal:kinetic:Poynting) $\sim$20:3:3 in the near tail, 12:4:3 in the middle tail, and 5:3:1 in the distant tail. Therefore the decrease of the energy flux is due to that of its thermal component, which is dominant throughout the magnetotail. The decrease of thermal energy flux in the near tail was mainly due to the decrease in the number density of plasma, while the decrease in the transition from the middle to distant tail was due to the decrease of ion temperature.

The dominance of the thermal component found above contradicts previous studies [e.g., *Scholer et al.*, 1984], in which the kinetic component was the dominant term. This difference is primarily due to the higher temperature found in this study. Note also that in previous studies, energy densities of plasmoids, not the energy flux, were used in the discussion of energy transport by plasmoids. The difference is that the factor of the thermal component was not 5/2 (thermal energy flux) but rather 3/2 (thermal energy density), and the Poynting component was described as $B^2/2\mu_0$ (magnetic energy density) in that case. Since one of our goals was to discuss substorm energetics, the energy flux of plasmoids, not energy density, was considered in this paper.

7. Discussion

In this section, we first discuss and estimate the dimensions of plasmoids in the middle and distant tail. Then the energy transported by plasmoids in the middle tail will be estimated, and its implication for the substorm energetics will be discussed.

7.1. Plasmoid Dimensions

The $Y_{\mathrm{GSM'}}$ and $Z_{\mathrm{GSM'}}$ dimensions of each plasmoid cannot be estimated from single satellite observations. Dimensions of plasmoids were remotely inferred by S93 from ISEE 3 observations of TCRs. They suggested that the typical size of a plasmoid was $35 \, R_E$ (length) $\times$ $15 \, R_E$ (width) $\times$ $15 \, R_E$ (height) in the middle and distant tail. The size of $\sim 15 \, R_E$ in the dawn-to-dusk direction was derived by S93 from the result that most TCRs were observed over a region 10-20 R_E wide. On the other hand, our results, as well as MH92, show that plasmoids are observed everywhere in the middle and distant tail. In this study, the $Y_{\mathrm{GSM'}}$ dimensions of plasmoids (L_y) were statistically estimated to be $\sim 20 \, R_E$ in the near tail and $\sim 40 \, R_E$ in the middle and distant tail. One possible interpretation for this discrepancy is that in the flank region the plasmoids are thin, so that TCRs are not clearly identified. An alternative interpretation is that in the flank region ISEE 3 was located in the region where plasmoids rather than TCRs were favorably observed.

We estimated plasmoid thickness in the $Z_{\mathrm{GSM'}}$ direction (L_z) by the method proposed by S93. Conservation of total magnetic flux in the tail lobe for the quiet time and during the passage of a plasmoid is described as

$$B_L S = B_{\mathrm{TCR}} (S - L_y \Delta H) \qquad (2)$$

where B_L and B_{TCR} are absolute values of the magnetic field of the quiet lobe and of the peak of a TCR. S is the quiet-time area of the tail lobe in the YZ plane, which is $\pi R^2 - 2RH$. (R is the radius of the magnetotail and H is the quiet-time thickness of the plasma sheet). L_y is the width of the plasmoid. ΔH is an increase in the thickness from the quiet-time plasma sheet to the plasmoid. Equation (2) yields $\Delta H \approx 110/L_y$, using $R \approx 24 \, R_E$ and $H \approx 2 \times 3.4 \, R_E$ as determined by *Fairfield* [1992], and $(B_{\mathrm{TCR}} - B_L)/B_L \approx 8\%$ by S93. Our result of $L_y \approx 40 \, R_E$ in the middle and distant tail yields $L_z = H + \Delta H \approx 10 \, R_E$, which is comparable to L_x presented before.

7.2. Energies Transported by a Plasmoid

We estimated the energy transported by a plasmoid using the energy flux and the dimensions of plasmoids obtained earlier. First, by calculating the product of the average energy flux and the duration of events, the energy transported by plasmoids through the unit area of $Y_{\mathrm{GSM'}} \times Z_{\mathrm{GSM'}}$ can be obtained and is shown in Figure 14. In the central region, the transported energy was nearly constant ($5 \times 10^{11} \, \mathrm{J}/R_E^2$) in the near and middle tail. It decreased from the middle tail to the distant tail to $2 \times 10^{11} \, \mathrm{J}/R_E^2$ and then was nearly constant in the distant tail. In the flank region, the energy was slightly smaller ($4 \times 10^{11} \, \mathrm{J}/R_E^2$) in the near and middle tail but slightly higher ($2.5 \times 10^{11} \, \mathrm{J}/R_E^2$) in the distant tail, compared with the central region.

Furthermore, to discuss the variations of energy carried by plasmoids, the variation of the cross section of plasmoids in the GSM' YZ plane must be considered. The cross sections of plasmoids increase from the near to middle tail because the widths of plasmoids increase.
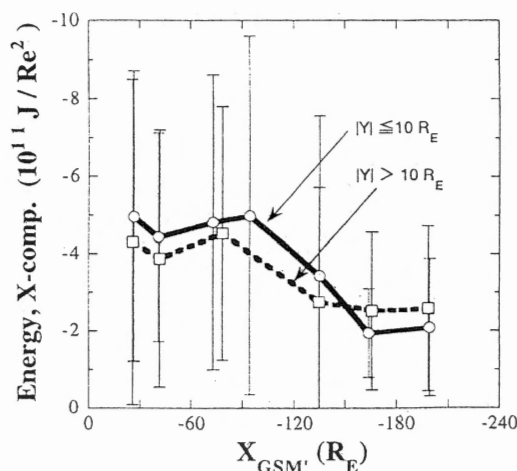
Figure 14. The $X_{\mathrm{GSM'}}$ component of the energy transported by plasmoids through an unit cross section.

Therefore the net energy transported by plasmoids increases with downtail distance from the near tail to the middle tail, possibly due to the energy supply from the NENL. The cross section seemed to be nearly constant from the middle tail to the distant tail. Therefore energy transported by plasmoids decreases and half is lost during the passage to the distant tail, possibly due to interactions with the surrounding medium.

To estimate the typical energy transported by a plasmoid, the parameters at $X_{GSM'} \approx -90\,R_E$ were used as representative values. This is because plasmoids at this position are in a situation just before energy loss in the transition from the middle tail to the distant tail. We have estimated that plasmoids have dimensions of $L_x \approx 10\,R_E$, $L_y \approx 40\,R_E$, and $L_z \approx 10\,R_E$. Assuming that plasmoids have the form of a cylinder, the volume of a plasmoid is $3 \times 10^3\,R_E^3$. The energy transported through the unit cross section was typically $5 \times 10^{11}\,J/R_E^2$, which was derived averaging the values in the central and the flank region with an assumption of the ratio of ion temperature to electron temperature to be 10. Then the energy transported by a plasmoid was calculated to be $\sim 16 \times 10^{13}\,J$.

7.3. Substorm Energetics

We estimated the energy transported by each plasmoid to be $\sim 16 \times 10^{13}\,J$. However, this value does not represent the whole tailward energy released in a substorm: First, plasmoids often appear as multiple events. From a study of TCR by S93, we can deduce that roughly 1.8 plasmoids are ejected in a substorm. Therefore energy transported by plasmoids in a tailward fast flow can be $\sim 3 \times 10^{14}\,J$.

Second, other portions of tailward fast flow must be included. Since their volume is unknown, their contributions to the energy transport of the whole tailward fast flow cannot be directly calculated. Here we will roughly estimate them. The energetic contribution by PSBL and pre-PPS is likely to be negligible: The ion temperature in the PSBL is lower, and the flow speed in the pre-PPS is slower than in plasmoids, and the volumes of PSBL and pre-PPS may be relatively small. However, it is likely that post-PPSs have a significant energy contribution to substorms. *Richardson et al.*

[1987] reported that post-PPSs had a typical velocity of 840 km/s. If the duration is 30 min, the "length" of post-PPS can be $240\,R_E$. Assuming that the width and the thickness of post-PPS are $10\,R_E \times 5\,R_E$, we obtain that a volume of a post-PPS is $\sim 12 \times 10^3\,R_E^3$. Since the energy flux in post-PPSs seems comparable to that in plasmoids, each post-PPS may contribute another $\sim 6 \times 10^{14}\,J$. Therefore energy contribution by post-PPSs can be greater than those due to plasmoids. As a consequence, the total energy carried by a tailward fast flow is roughly $\sim 10^{15}\,J$.

Kamide and Baumjohann [1993] discussed substorm energetics. They suggested rough equipartition of energy in a substorm among the auroral ionosphere, ring current, and plasmoid, with a typical value of $10^{15}\,J$ for each region. This value is consistent with our results. Therefore it is confirmed that plasmoid-associated tailward fast flow has a significant energetic contribution to substorms, which supports the NENL model.

8. Summary and Conclusions

We have defined a plasmoid as an individual magnetic loop, in which the total pressure enhancement (TPE) is a necessary condition. After showing three examples of plasmoids, we have reported on the qualitative and quantitative nature of plasmoids. The energy transported by plasmoids has been estimated, and furthermore substorm energetics have been briefly discussed. Characteristic plasmoid parameters found in this study are summarized in Table 1. On the basis of Geotail observations of plasmoids, the three-dimensional picture of plasmoids and their evolution along the downtail direction on the equatorial plane are estimated as follows and schematically illustrated in the GSM' XY plane in Figure 15.

1. In the near tail, plasmoids rapidly accelerated in the downtail direction and expanded in the $Y_{GSM'}$ direction. A drop in ion density and nearly constant ion temperatures were found. The $X_{GSM'}$ dimension of plasmoids is $4\,R_E$ around $X_{GSM'} \approx -30\,R_E$. Plasmoids are localized with a width of $\sim 20\,R_E$ in $Y_{GSM'}$. Most plasmoids were observed beyond $X_{GSM'} \approx -25\,R_E$. The center of plasmoids in the near tail, and possi-

Table 1. Basic Quantities of Plasmoids

Quantity	$-16 > X \geq -30$	$-30 > X \geq -50$	$-50 > X \geq -100$	$-100 > X \geq -210$
Average $X_{GSM'}$, R_E	-26	-40	-81	-172
Number of plasmoids	110	106	157	451
V_x, km/s	-350 ± 150	-470 ± 230	-680 ± 270	-590 ± 240
Density, cm^{-3}	0.25 ± 0.14	0.15 ± 0.10	0.08 ± 0.07	0.11 ± 0.10
T_i, keV	4.4 ± 1.7	4.4 ± 2.3	4.8 ± 2.4	2.0 ± 1.3
$|B|$, nT	10 ± 4	9 ± 4	7 ± 3	5 ± 2
Duration, min	1.2 ± 0.4	1.3 ± 0.5	1.7 ± 0.7	1.8 ± 0.7
L_x, R_E	4 ± 2	6 ± 3	10 ± 5	10 ± 5
Energy flux, $10^9\,W/R_E^2$	-7 ± 5	-6 ± 4	-4 ± 3	-3 ± 2

Basic quantities of plasmoids and their standard deviations are summarized against $X_{GSM'}$ (R_E).
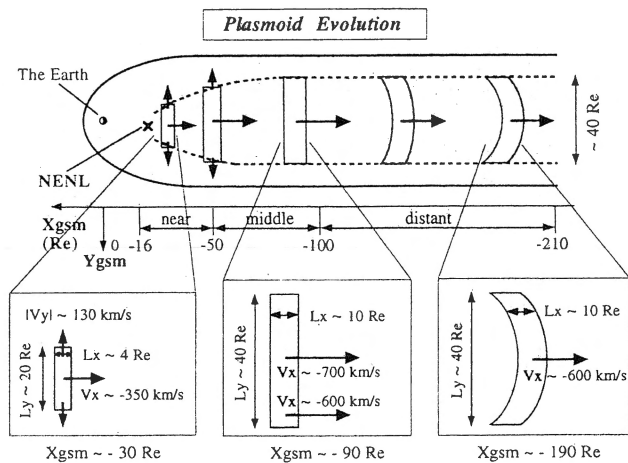
Figure 15. Schematic illustration of plasmoid evolution from the near to the distant tail in the aberrated GSM XY plane. Typical velocities, dimensions, and forms in the near, the middle, and the distant tail are displayed in the three expanded portions.

bly that of the NENL, are likely to be located around $Y_{GSM'} = 3\,R_E$. In Figure 15, the NENL is shown as a cross with its location assumed to be $X_{GSM'} \approx -21\,R_E$.

2. In the middle tail, a weak expansion seemed to remain. The density was nearly constant and the ion temperature was still high, which suggested that the NENL was still active. Typical plasmoid dimensions were estimated to be $10\,R_E$ (length) $\times 40\,R_E$ (width) $\times 10\,R_E$ (height).

3. In the transition from the middle to distant tail, plasmoids began to decelerate and the ion temperature rapidly decreased. About half of the energy transported by plasmoids will be lost in this transition by a nonadiabatic mechanism.

4. In the distant tail, the density was nearly constant in the central region and slightly increased in the flank region. Typical plasmoid dimensions were estimated to be nearly the same as in the middle tail. As a consequence of lower speed in the flank region, it is expected that plasmoids are deformed with a typical scale length comparable to the length of the plasmoid.

The energetics of plasmoids were also discussed. The thermal component was dominant throughout the magnetotail from $X_{GSM'} = -16$ down to $-210\,R_E$. The energy transported by each plasmoid was estimated to be $\sim 2 \times 10^{14}\,$J in the middle tail. Energy released tailward in a substorm was inferred to be $\sim 10^{15}\,$J, which is the same order as the energy released to the auroral region and to the ring current in support of the NENL model.

References

Baker, D. N., T. I. Pulkkinen, V. Angelopoulos, W. Baumjohann, and R. L. McPherron, Neutral line model of substorms: Past results and present view, *J. Geophys. Res.*, *101*, 12,975-13,010, 1996.

Fairfield, D. H., On the structure of the distant magnetotail: ISEE 3, *J. Geophys. Res.*, *97*, 1403-1410, 1992.

Gloeckler, G., F. M. Ipavich, D. Hovestadt, M. Scholer, A. B. Galvin, and B. Klecker, Characteristics of suprathermal H^+ and He^{++} in plasmoids in the distant magnetotail, *Geophys. Res. Lett.*, *11*, 1030-1033, 1984.

Hones, E. W., Jr., The magnetotail: Its generation and dissipation, in *Physics of Solar Planetary Environments*, edited by D. J. Williams, pp. 559-571, AGU, Washington, D. C., 1976.

Hones, E. W., Jr., D. N. Baker, S. J. Bame, W. C. Feldman, J. T. Gosling, D. J. McComas, R. D. Zwickl, J. A. Slavin, E. J. Smith, and B. T. Tsurutani, Structure of the magnetotail at 220 R_E and its response to geomagnetic activity, *Geophys. Res. Lett.*, *11*, 5-8, 1984a.

Hones, E. W., Jr., J. Birn, D. N. Baker, S. J. Bame, W. C. Feldman, D. J. McComas, and R. D. Zwickl, Detailed examination of a plasmoid in the distant magnetotail with ISEE 3, *Geophys. Res. Lett.*, *11*, 1046-1049, 1984b.

Hughes, W. J., and D. G. Sibeck, On the three-dimensional structure of plasmoids, *Geophys. Res. Lett.*, *14*, 636-639, 1987.

Kamide, Y., and W. Baumjohann, *Magnetosphere-Ionosphere Coupling*, p. 10, Springer-Verlag, New York, 1993.

Kokubun, S., T. Yamamoto, M. H. Acuña, K. Hayashi, K. Shiokawa, and H. Kawano, The Geotail magnetic field experiment, *J. Geomagn. Geoelectr.*, *46*, 7-21, 1994.

Lee, L. C., S. Wang, C. Q. Wei, and B. T. Tsurutani, Streaming sausage, kink and tearing instabilities in a current sheet with applications to the Earth's magnetotail, *J. Geophys. Res.*, *93*, 7354-7365, 1988.

Machida, S., T. Mukai, Y. Saito, T. Obara, T. Yamamoto, A. Nishida, M. Hirahara, T. Terasawa, and S. Kokubun, Geotail low-energy particle and magnetic field observations of a plasmoid at $X_{GSM} = -142\,R_E$, *Geophys. Res. Lett.*, *21*, 2995-2998, 1994.

Maezawa, K., Magnetotail boundary motion associated with geomagnetic substorms, *J. Geophys. Res.*, *80*, 3543-3548, 1975.

Moldwin, M. B., and W. J. Hughes, On the formation and evolution of plasmoids: A survey of ISEE 3 geotail data, *J. Geophys. Res.*, *97*, 19,259-19,282, 1992a.

Moldwin, M. B., and W. J. Hughes, Multisatellite observations of plasmoids: IMP 8 and ISEE 3, *Geophys. Res. Lett.*, *19*, 1081-1084, 1992b.

Moldwin, M. B., and W. J. Hughes, Geomagnetic substorm association of plasmoids, *J. Geophys. Res.*, *98*, 81-88, 1993.

Mukai, T., S. Machida, Y. Saito, M. Hirahara, T. Terasawa, N. Kaya, T. Obara, M. Ejiri, and A. Nishida, The Low Energy Particle (LEP) experiment onboard the Geotail satellite, *J. Geomagn. Geoelectr.*, *46*, 669-692, 1994.

Nagai, T., K. Takahashi, H. Kawano, T. Yamamoto, S. Kokubun, and A. Nishida, Initial Geotail survey of magnetic substorm signatures in the magnetotail, *Geophys. Res. Lett.*, *21*, 2991-2994, 1994.

Nishida, A., The Geotail mission, *Geophys. Res. Lett.*, *21*, 2871-2873, 1994.

Nishida, A., M. Scholer, T. Terasawa, S. J. Bame, G. Gloeckler, E. J. Smith, and R. D. Zwickl, Quasi-stagnant plasmoid in the middle tail: A new preexpansion phase phenomenon, *J. Geophys. Res.*, *91*, 4245-4255, 1986.

Nishida, A., T. Mukai, Y. Saito, T. Yamamoto, H. Hayaka-

wa, K. Maezawa, S. Machida, T. Terasawa, S. Kokubun, and T. Nagai, Transition from slow flow to fast tailward flow in the distant plasma sheet, *Geophys. Res. Lett.*, *21*, 2939-2942, 1994.

Richardson, I. G., S. W. H. Cowley, E. W. Hones Jr., and S. J. Bame, Plasmoid-associated energetic ion bursts in the deep geomagnetic tail: Properties of plasmoids and the postplasmoid plasma sheet, *J. Geophys. Res.*, *92*, 9997-10,013, 1987.

Scholer, M., G. Gloeckler, D. Hovestadt, B. Klecker, and F. M. Ipavich, Characteristics of plasmoidlike structures in the distant magnetotail, *J. Geophys. Res.*, *89*, 8872-8876, 1984.

Slavin, J. A., E. J. Smith, D. G. Sibeck, D. N. Baker, R. D. Zwickl, and S. -I. Akasofu, An ISEE 3 study of average and substorm conditions in the distant magnetotail, *J. Geophys. Res.*, *90*, 10,875-10,895, 1985.

Slavin, J. A., et al., CDAW 8 observations of plasmoid signatures in the geomagnetic tail: An assessment, *J. Geophys. Res.*, *94*, 15,153-15,175, 1989.

Slavin, J. A., M. F. Smith, E. L. Mazur, D. N. Baker, E. W. Hones Jr., T. Iyemori, and E. W. Greenstadt, ISEE 3 observations of traveling compression regions in the Earth's magnetotail, *J. Geophys. Res.*, *98*, 15,425-15,446, 1993.

Tsurutani, B. T., M. E. Burton, E. J. Smith, and D. E. Jones, Statistical properties of magnetic field fluctuations in the distant plasmasheet, *Planet. Space Sci.*, *35*, 289-293, 1987.

Weiss, L. A., P. H. Reiff, J. J. Moses, R. A. Heelis, and B. D. Moore, Energy dissipation in substorms, in *Proceedings of the First International Conference on Substorms, Eur. Space Agency Spec. Publ.*, *ESA SP-335*, 309-317, 1992.

A. Ieda and S. Machida, Department of Earth and Planetary Science, Kyoto University, Kyoto 606-01, Japan. (e-mail: ieda@kugi.kyoto-u.ac.jp; machida@kugi.kyoto-u.ac.jp)

S. Kokubun, Solar Terrestrial Environment Laboratory, Nagoya University, Toyokawa, Aichi 441, Japan. (e-mail: kokubun@stelab.nagoya-u.ac.jp)

T. Mukai, A. Nishida, Y. Saito, and T. Yamamoto, Institute of Space and Astronautical Science, 3-1-1, Yoshinodai, Sagamihara, Kanagawa 229, Japan. (e-mail: mukai@gtl.isas.ac.jp; nishida@gtl.isas.ac.jp; saito@gtl.isas.ac.jp; yamamoto@gtl.isas.ac.jp)

T. Terasawa, Department of Earth and Planetary Physics, University of Tokyo, Hongo, Tokyo 113, Japan. (e-mail: terasawa@grl.s.u-tokyo.ac.jp)